Biotoxoid photonic sensors with temperature insensitivity using a cascade of ring resonator and Mach–Zehnder interferometer

Li, Zhenyu; Zou, Jun; Zhu, Huihui; Nguyen, Binh Thi Thanh; Shi, Yuzhi; Liu, Patricia Yang; Bailey, Ryan C.; Zhou, Jin; Wang, Hong; Yang, Zhenchuan; Jin, Yufeng; Yap, Peng Huat; Cai, Hong; Hao, Yilong; Liu, Ai Qun

2020

Li, Z., Zou, J., Zhu, H., Nguyen, B. T. T., Shi, Y., Liu, P. Y., Bailey, R. C., Zhou, J., Wang, H., Yang, Z., Jin, Y., Yap, P. H., Cai, H., Hao, Y. & Liu, A. Q. (2020). Biotoxoid photonic sensors with temperature insensitivity using a cascade of ring resonator and Mach–Zehnder interferometer. ACS Sensors, 5(8), 2448-2456.
https://dx.doi.org/10.1021/acssensors.0c00622

https://hdl.handle.net/10356/151457

https://doi.org/10.1021/acssensors.0c00622

A Biotoxoid Photonic Sensor with Temperature-Insensitivity Using Cascade of Ring Resonator and Mach-Zehnder Interferometer

Zhenyu Li[1,2], Jun Zou[2*], Huihui Zhu[2], Binh Thi Thanh Nguyen[2], Yuzhi Shi[2], Patricia Yang Liu[2], Ryan C. Bailey[3], Jin Zhou[2], Hong Wang[2], Zhenchuan Yang[1], Yufeng Jin[1], Peng Huat Yap[4], Hong Cai[5*], Yilong Hao[1*] and Ai Qun Liu[2*]

[1]*National Key Laboratory of Science and Technology on Micro/Nano Fabrication, Institute of Microelectronics, Peking University, Beijing 100871, China*

[2]*Quantum Science and Engineering Centre, Nanyang Technological University, 50 Nanyang Avenue, Singapore 639798, Singapore*

[3]*Department of Chemistry, University of Michigan, 930 North University Avenue, Ann Arbor, Michigan 48109, United States*

[4]*Lee Kong Chian School of Medicine, Nanyang Technological University, Singapore 308232, Singapore*

[5]*Institute of Microelectronics, A*STAR (Agency for Science, Technology and Research), Singapore 138634, Singapore*

[*]*Corresponding Author: zoujun@ntu.edu.sg, caih@ime.a-star.edu.sg, haoyl@pku.edu.cn, eaqliu@ntu.edu.sg*

Abstract

The great advances in silicon photonic sensing technology have made it an attractive platform for a wide of sensing applications. However, most silicon photonic sensing platforms suffer from high susceptibility to the temperature fluctuation of operating environment. Additional complex and costly chemical signal enhancement strategies are usually required to improve the signal-to-noise ratio (SNR). Here, a biotoxoid photonic sensor that is resistant to temperature fluctuation have been demonstrated. This novel sensor consists of a ring resonator coupled to a Mach-Zehnder interferometer (MZI) readout unit. Instead of using costly wavelength interrogation, our photonic sensor directly measures the light intensity ratio between the two output ports of MZI. The temperature dependence (TD) controlling section of the MZI is used to eliminate the adverse effects of ambient temperature fluctuation. The simulation and experimental results show a linear relationship between the interrogation function and the concentration of analyte under operation conditions. The thermal drift of the proposed sensor is just 0.18%, which is a reduction of 567 folds for chemical sensing and 28 folds for immuno-biosensing compared to conventional single ring resonator. The SNR increases from 6.85 dB to 19.88 dB within a 2°C temperature variation. The high SNR optical sensor promises great potential for amplification-free of detection of nucleic acids and other biomarkers.

Keywords: biotoxoid detection; silicon photonic sensor; ring resonator; MZI; temperature insensitivity; intensity integration.

In recent years, silicon photonic ring resonator-based sensor has been widely applied to the detection of various chemical and biological analytes, such as proteins, RNA and other biomarkers[1-7]. Compared to other detection platforms, the silicon ring resonator has numerous advantages such as high sensitivity, compact size, label-free sensing scheme, real-time readout, low sample consumption, multiplexing and immunity to electromagnetic interference[8]. Moreover, the ring resonator is compatible with complementary metal oxide semiconductor (CMOS) processing, which enables mass production and easy integration with on-chip light sources, detectors and microfluidic units, leading to a multi-functional platform for the detection of various chemical or biological components[9-10].

Despite its many advantages, one common problem with the silicon ring resonator is that the output spectrum constantly drifts due to the fluctuation of ambient temperature. The detection accuracy is hence compromised by this temperature-induced signal drift, which could reach up to ~ 50 pm/°C for silicon-based ring resonator due to its large thermal-optic (TO) coefficient (1.86×10^{-4} /K)[11-12]. Recently, several strategies have been proposed to enhance the sensitivity of ring resonators. For instance, the Vernier effect, which explores the tiny difference between free spectral ranges (FSR) of the sensing and reference ring resonators, has significantly improved the sensitivity and limit of detection (LOD)[13-14]. Nevertheless, the temperature-induced wavelength drift can also be amplified by the Vernier effect and superimposed on top of the true signals, which would significantly decrease the signal-to-noise ratio (SNR) and compromise the advantage of the Vernier effect. Therefore, eliminating the adverse effect resulting from temperature fluctuation is of ultimate importance to a reliable silicon ring resonator-based sensor. A

number of methods have been developed to tackle this problem. One approach is to maintain a constant temperature on chip with a temperature controller[15]. However, it takes a long time for the temperature to stabilize whenever a new reagent is introduced to the resonator. In addition, it is difficult to integrate the temperature controller on a silicon photonic chip. Another approach incorporates a reference ring resonator to monitor the temperature variability in real time[16]. In this case, extra data processing is required to correct the temperature effect, and each detection ring must be accompanied by a reference ring due to the temperature variability on chip, which would significantly complicate the chip design and operation. Yet another method is to fabricate athermal structures using materials with opposite thermal-optic coefficients in core and cladding regions[17]. However, it is challenging to identify appropriate materials that are compatible with existing fabrication processes. In addition to the effort in improving the resonator chip structure, new assay formats have also been implemented to achieve high sensitivity. For instance, additional binding agents are introduced to generate multi-layer stacks of biomolecule on the ring resonator to enhance the signal. The binding agents could also be conjugated to enzymes that promote the generation of insoluble substrate that precipitates on the ring resonator for signal enhancement., Although these methods are effective, they are complex and highly costly[18-19].

The signal readout of ring resonators primarily relies on wavelength interrogation. However, wavelength interrogation usually requires a costly and bulky tunable laser source with a super-narrow linewidth or a high-resolution optical spectrum analyzer (OSA) due to the high Q value of the resonant peak in the spectrum[20]. To tackle this problem, a low-cost broadband source is used to excite the sensing ring, and on-chip

spectrometers such as arrayed waveguide gratings (AWGs) are employed to interrogate the wavelength shift of the resonant peak[21-22]. A high-resolution on-chip spectrometer is required to achieve high detection sensitivity. However, such an on-chip spectrometer would lead to a significant increase in chip size.

Because of the aforementioned limitations, it is challenging but highly desired to develop a simple and reliable integrated photonic sensing system for the detection of biotoxins, RNA and other biomarkers. In this paper, a temperature-insensitive biotoxoid photonic sensor that combines a ring resonator and a Mach-Zehnder interferometer (MZI) is demonstrated to detect botulinum toxoid type A. A low-cost broadband light source is used as the input of the sensing ring, and the output signal is interrogated by detecting the light intensity ratio between the two output ports of the MZI. A temperature-dependent section embedded in the two arms of the MZI is designed to correct the spectrum drift due to temperature fluctuation. We demonstrate glucose sensing based on refractive index and quantitative detection of botulinum toxoid type A using an immunoassay. The adverse effect due to thermal drift of the proposed sensor is reduced by 567 times for glucose sensing and by 28 times for botulinum toxoid type A detection compared to the single ring resonator sensor. The SNR increases from 6.85 dB to 19.88 dB within 2°C variation.

Design and Theoretical Analysis

Figure 1(a) shows a schematic illustration of the photonic sensor consisting of a ring resonator and an MZI with temperature dependence (TD) control sections embedded in both arms. A broadband light source is coupled into the bus waveguide through an input fiber to excite the sensing ring, and a resonant peak emerges at its drop port. The

resonant peak is then launched into the input of the MZI, *i.e.* a Y-splitter, by which the input light is divided into two sub-beams of equal intensity. After propagating along different paths, these two sub-beams pass through a directional coupler (DC). Finally, intensity signals from the two output ports of the DC are acquired by two photodetectors.

As shown in Figure 1(a), the sensing ring comprises two DCs with self-coupling and cross-coupling coefficients of r_i and k_i (i = 1, 2), respectively, and $r_i^2 + k_i^2 = 1$. The waveguide width w_s of the ring resonator is optimized for high sensitivity and large fabrication tolerance. The transmittance function of the drop-port is expressed as[23]

$$T_d(\lambda) = \frac{I_d}{I_{in}} = \frac{\left(1-r_1^2\right)\left(1-r_2^2\right)a}{1-2r_1r_2a\cos(2\pi n_{eff}L_r/\lambda)+(r_1r_2a)^2} \quad (1)$$

where $a^2 = exp\,(-\alpha L_r)$ is the single-pass transmission loss, including both propagation loss in the ring and loss in the couplers. α is the power attenuation coefficient, L_r is circumference of the ring, and n_{eff} is effective index of the guiding mode in the ring.

The MZI with two output ports O_1 and O_2 consists of two sections as shown in Figure 1(a). One section has a normal MZI design with waveguide width of w_0 same as the ring resonator and lengths of L_1 and L_2 for the upper and lower arms, respectively. The length difference between the two arms is defined as $\Delta L = L_1 - L_2$. The other is the TD adjusting section with a narrow waveguide of width w_1, a wide waveguide of width w_2 and a length of $L_a = x \cdot \Delta L$, where x is defined as the TD compensation factor. When x = 0, it is a conventional MZI without the TD adjusting section. When $x > 0$, the wide waveguide is located in the lower arm of the MZI, as the case illustrated in Figure 1(a). In contrast, the wide waveguide is located in the upper arm when $x < 0$. Assuming that the output DC of the MZI structure has a cross-coupling coefficient of k_m, the transmittance functions for the two output ports of the MZI are written as

$$T_{O_1}(\lambda) = \frac{I_{O_1}}{I_{in}} = \frac{1}{2}(1 + 2k_m \cdot \sqrt{1 - k_m{}^2} \cdot \sin\Phi) \tag{2a}$$

$$T_{O_2}(\lambda) = \frac{I_{O_2}}{I_{in}} = \frac{1}{2}(1 - 2k_m \cdot \sqrt{1 - k_m{}^2} \cdot \sin\Phi) \tag{2b}$$

$$\Phi = \frac{2\pi \cdot \Delta L}{\lambda}\left[n_{eff}(w_0) + x \cdot \left(n_{eff}(w_1) - n_{eff}(w_2) \right) \right] \tag{2c}$$

where $n_{eff}(w_0)$, $n_{eff}(w_1)$ and $n_{eff}(w_2)$ are effective indices of the normal waveguide, narrow waveguide and wide waveguide, respectively.

Assuming that the sensing ring resonates at a wavelength λ_s, and in combination with the transmittance functions of the ring resonator and MZI, the final output signals from the two output ports O_1 and O_2 of the sensing system are expressed as

$$I_{O_1}(\lambda_s) = \int_{\lambda_-}^{\lambda_+} S(\lambda) \cdot T_d(\lambda) \cdot T_{O_1}(\lambda) d\lambda \tag{3a}$$

$$I_{O_2}(\lambda_s) = \int_{\lambda_-}^{\lambda_+} S(\lambda) \cdot T_d(\lambda) \cdot T_{O_2}(\lambda) d\lambda \tag{3b}$$

where $S(\lambda)$ is the emission spectrum of the input light source with a wavelength ranging from λ_- to λ_+. It is noted that if the broadband light source $S(\lambda)$ covers multiple resonant peaks of the sensing ring in its response spectrum, the value of I_{Oi} (i = 1, 2) by intensity interrogation will be significantly altered, resulting in a large detection error. In order to address this problem, the solution is to design a sensing ring with an FSR larger than the spectral width of the input broadband source, which will result in only one resonant peak at its drop-port. An alternative method is to ensure that only one resonant peak would appear in the response spectrum by limiting the input bandwidth with a wavelength filter.

An interrogation function $R(\lambda_s)$ is defined for the resonant wavelength of the sensing ring resonator. $R(\lambda_s)$ is obtained by taking the logarithm of the power ratio between the two outputs O_1 and O_2, which is expressed as

$$R(\lambda_s) = 10\lg\frac{I_{O_1}(\lambda_s)}{I_{O_2}(\lambda_s)} \tag{4}$$

Since the light source $S(\lambda)$ is included in the integral term of both Eqs. (3a) and (3b), it can be deduced that the value of $R(\lambda_s)$ is independent on the power fluctuation of $S(\lambda)$. According to Eqs. (2a) and (2b), the output T_{Oi} of the MZI is dependent on the DC cross-coupling coefficient k_m, hence the interrogation function is also a function of k_m. Figure 2(a) shows the spectral responses of the two outputs O_1 and O_2 of the MZI when $k_m = \sqrt{0.1}$, $\sqrt{0.2}$, $\sqrt{0.3}$, $\sqrt{0.4}$ and $\sqrt{0.5}$ with FSR_m of the MZI being 5 nm. It is noticed that $T_{O1}(\lambda)$ and $T_{O2}(\lambda)$ have different values when k_m is different. $R(\lambda_s)$ as a function of wavelength λ_s is shown in Figure 2(b) with an enlarged view showing the wavelength range around 1550 nm in the inset. The linear range between R and λ_s increases with increasing k_m (limited to $k_m < \sqrt{0.5}$), but decreases as k_m further increases. In the linear region, the slope of R with respect to λ_s indicates the detection sensitivity and increases with the increasing k_m (limited to $k_m < \sqrt{0.5}$). Therefore, there is a tradeoff between the linear range and sensitivity. In the following design, we set k_m to $\sqrt{0.2}$, which corresponds to a large linear dynamic range that corresponds to ~ 70% of the half of FSR_m of the MZI.

Figure 1(b) shows the schematics of the temperature-insensitive detection by the ring resonator when the ambient temperature drifts by a small degree ΔT. For clarity, we assume that the temperature variability results in a shift of resonant wavelength by $\Delta\lambda_{Ts}$ and $\Delta\lambda_{Tm}$ for the ring resonator and MZI, respectively. The initial value of R is assumed to be R_0 before the temperature changes by ΔT. As shown in Figure 1(b), for R to remain constant under temperature fluctuations, $\Delta\lambda_{Tm} = \Delta\lambda_{Ts}$ must be satisfied, a scenario known as on-compensation. As shown in Figure 1(b), if $\Delta\lambda_{Tm} < \Delta\lambda_{Ts}$, the value of R becomes

larger, a scenario known as under-compensation. In contrast, if $\Delta\lambda_{Tm} > \Delta\lambda_{Ts}$, the value of R becomes smaller, a scenario known as over-compensation. Therefore, in order to eliminate the error resulting from temperature fluctuation, the relationship of $\Delta\lambda_{Tm} = \Delta\lambda_{Ts}$ should always be satisfied, *i.e.* the TD of the MZI must be the same as that of the sensing ring. During sensing, the sensing ring and the reference ring should be kept in the same thermal environment by being placed in the same microfluidic channel[24].

Since silicon has a large TO coefficient, the temperature variability significantly influences the spectral response of silicon-based devices. The TD of the sensing ring resonator, *i.e.* its resonant wavelength shift with respect to temperature change, is written as

$$\frac{\partial \lambda_s}{\partial T} = \frac{\partial n_{eff}}{\partial T} \cdot \frac{\lambda_s}{n_g} \tag{5}$$

where $n_g = n_{eff} - \lambda \cdot dn_{eff}/d\lambda$ is group index of the fundamental guiding mode in the ring waveguide. Similarly, for the MZI in Figure 1(a),

$$\frac{\partial \lambda_m}{\partial T} = \frac{\lambda_m}{n_g(w_0) + \left(n_g(w_1) - n_g(w_2)\right) \cdot x} \times \left(\frac{\partial n_{eff}(w_0)}{\partial T} + \left(\frac{\partial n_{eff}(w_1)}{\partial T} - \frac{\partial n_{eff}(w_2)}{\partial T} \right) \cdot x \right) \tag{6}$$

where $n_g(w_i) = n_{eff}(w_i) - \lambda_m \cdot dn_{eff}(w_i)/d\lambda$ (i = 0, 1, 2) is the group index of the fundamental mode of the waveguide with width w_i. Given in Eqs. (5) and (6), the TDs are mainly attributed to effective index changes of the fundamental modes in the ring and MZI waveguides with respect to temperature variability, i.e., $\partial n_{eff}/\partial T$, which is determined by the waveguide dimension, operating wavelength and TO coefficient of the upper-cladding material. Furthermore, it is seen from Eq. (6) that the second term in parentheses on the right-hand side denotes the TD adjusting parameters. Therefore, TD of the MZI can be altered by adjusting the width of the narrow and broad waveguide by a

constant x or by adjusting the compensation factor x when the widths of the MZI arms remain constant.

Thermal expansion of silicon affects the effective index n_{eff} of the guiding mode in the waveguide, which is the major reason for temperature susceptibility of silica-on-silicon platform-based devices[25]. However, it is negligible compared to the TO effect of silicon[26]. Therefore, we only consider the TO effect of silicon on n_{eff} of the guiding mode, and use Eqs. (5) and (6) to analyze TDs of the sensing ring and MZI, respectively.

The advantage of the proposed sensor structure is that the sensing ring resonator and MZI can be designed and optimized independently. Therefore, the sensing ring resonator can be designed with a high sensitivity and a large tolerance for easy fabrication. The MZI, on one hand, is designed to match the TD of the sensing ring to realize temperature-insensitive detection. On the other hand, it is also optimized to obtain a wide linear dynamic range between the interrogation function $R(\lambda_s)$ and the resonant wavelength λ_s of the sensing ring in the required detection range.

Simulation Design. Here, we consider a SOI wafer with a top silicon layer with a thickness of 220 nm and buried oxide (BOX) layer of 3 μm. The finite-difference eigenmode (FDE) solver is used to calculate the effective index and group index of the fundamental guiding mode. The device is covered by an upper-cladding layer made of silicon dioxide with a thickness of 1.5 μm. The sensing ring is submerged in the sensing medium during detection. The sensing medium is the deionized (DI) water, which is pertinent to most biosensing applications. Refractive indices and TO coefficient of relevant materials at the wavelength of 1.55 μm are listed in Table S1.

Based on Eq. (5), TDs of the fundamental TE mode for a waveguide with water and SiO_2 as the upper-cladding are calculated in Figure 2(c). The TDs increase as the width of waveguide increases and gradually reach a plateau. When silica is used as the upper cladding of the waveguide, the TD is larger than the case with water as the upper cladding for the waveguide of the same width. The key to temperature-insensitive detection is to keep TD the same between the ring resonator and the MZI. Taking into account of the single mode condition in the sensing ring and large fabrication tolerance in MZI, we set the waveguide width to 450 nm for the sensing ring, and $w_1 = w_0 = 450$ nm and $w_2 = 800$ nm for the MZI arms. Fundamental mode of the normal width w_0 in MZI is adiabatically converted to that of the broad width w_2 by a taper section to avoid exciting higher-order modes. Table 1 summarizes relevant simulated results of the fundamental TE mode for the designed ring resonator and MZI waveguides operating at the wavelength of 1.55 μm. According to Eq. (6) and in combination with the simulated results in Table 1, TD of the MZI as a function of the compensation factor x is calculated and shown in Figure 2(d). The TD of MZI can be tuned to any value by altering x. When the MZI has the same TD as the sensing ring, the required value of x is approximately 2.43. Considering the deviation between the design and the fabricated device, three values of x (2, 2.43 and 3) are employed in our design.

Preparation and Methods

Chip Fabrication and Experimental Set-up. The sensing structure is fabricated on a SOI wafer based on the simulation. First, the 70-nm thick silicon is etched by inductively coupled plasma reactive ion etching to form grating couplers, and the remaining 150-nm Si is etched to define the wire waveguides. Subsequently, an upper-

cladding layer of 1.5-μm silica is deposited by plasma-enhanced chemical vapor deposition (PECVD). After that, the sensing window of the ring resonator is opened by anisotropic RIE dry etching and isotropic etching based on the vapor HF to remove the silica upper-cladding. The micrographs of the fabricated sensing chip are shown in Figures 3(a), 3(b) and 3(c) (More images about the setup and the device are available in Supplementary Figure S1). In the experiment, the sensing chip is packaged into a home-made holder with a microfluidic flow channel made by laminating a laser-cut gasket (perfluoroelastomer, Kalrez) over the sensing window of the ring resonator. An aluminum chip holder and lid are placed on top to hold the gasket in place, forming an integrated optofluidic system[27-30]. A temperature controller (TED 200 C, Thorlabs) is placed beneath the optofluidic system to control the temperature[31]. A broadband optical light source (ALS-CL-13-B-FA, Amonics) connected to an external bandwidth-variable tunable filter (BVF-200CL, Alnair Labs) generates a wavelength ranging from 1540 to 1550 nm, which ensures that only one resonant peak of the sensing ring is excited. The light source is tuned to TE polarization via a fiber polarization controller (FPC032, Thorlabs), and coupled into the bus waveguide through a fiber array with four channels. After propagating through the sensing chip, the output light from through-port O_0 of the sensing ring is coupled out of the chip via a grating coupler to an external OSA (AQ6370D, Yokogawa) as a reference to monitor the resonant peak shift of the sensing ring. The other two outputs O_1 and O_2 are connected to two photodetectors inside a multi-channel power meter (MPM-210, Santec) to monitor the output of MZI. The measured spectra from output ports O_0, O_1 and O_2 are shown in Figure 3(d). Due to fabrication imperfections, the dimension of the fabricated waveguide is slightly different from the

designed specifications, thereby resulting in a blue shift of the resonant wavelength of the sensing ring.

Detection Procedure. The sensing capability is first demonstrated by measuring the bulk refractive index of glucose solution of various concentrations (Sigma-Aldrich) [32]. The glucose solution is injected into the microfluidic channel by a syringe pump (neMESYS, CETONI GmbH). The solution flows through the bare surface of the sensing chip maintained at a constant temperature by the temperature controller. When the signal of the reference port O_0 becomes stable, the power signal from port O_1 and O_2 are collected for 30 seconds with 3 repeats. The same procedure is conducted at several different temperatures. Then the microfluidic channel is washed with DI water before another glucose concentration is injected. The detection for glucose with concentration ranging from 0 to 2.5% with a step of 0.5% is shown in Figure 4.

The botulinum toxoid type A (BoNT-A, DuoSet) is detected using the same chip design. The surface of the sensing ring is pre-functionalized with capture antibodies as shown in Figure 5(a). The sensor chip is rinsed with acetone and ethanol to remove surface contamination, and it is further cleaned with oxygen plasma (PDC-002, Harrick Plasma) for 5 min before being immersed into a 5% (*v/v*) solution of 3-aminopropyltriethoxysilane (APTES, Thermo Fisher Scientific) (2 mL in acetone, 4 min). After rinsing and drying, the salinized chip reacts with a 5 mM solution of the bis(sulfosuccinimidys)suberate (BS3, Thermo Fisher Scientific) cross linker (20 μL, 2 mg in 700 μL 2 mM acetic acid) for 3 min. After another round of rinsing and drying, the capture antibody (0.3 mg/mL) (DuoSet ELISA development system, R&D Systems) is immobilized on the waveguide surfaces of the sensing ring via covalent linkage.

Following antibody immobilization, the surface is passivated by the blocking buffer (StartingBlock, Thermo Fisher Scientific) and stored at 4°C for at least one hour before use. Before each measurement, the chip is loaded into the optofluidic holder. Baseline signal is obtained with running buffer (Ancillary Reagent Kit 2, DuoSet) that is injected at 30 μL/min for 2 minutes. After the signal from ports O_0 gets stable, the sample is injected into the microfluidic channel and interacts with the capture antibody that is pre-functionalized on the surface of the sensing ring for 20 minutes. The running buffer runs for another 2 minutes, and then the signal is collected. Subsequently, the sample is measured under different temperatures. Finally, the regeneration buffer is injected for around 30 seconds to release the sample from the capture antibody [33-35].

Experimental Results and Discussions

Performance Characterization Results. Figure 4(a) shows the TD results of the three sensors designed with x = 2, 2.43 and 3 at the temperature ranging from 20.0°C to 23.0°C with a step of 0.5°C. The TDs of these three sensors with compensation are reduced to a low level. And the sensor shows a lowest TD of 0.00058 /°C when x = 3. For comparison, we also deduce the TD of the sensing ring using the wavelength signal from Port O_0, which gives a TD of 0.329 /°C as shown in dash line. The value is 567 times larger than the compensated sensor when x = 3. Figure 4(b) shows the bulk refractive index sensing results with x = 2.43 for glucose solutions from 0.0% to 2.5% with a step of 0.5%. At the same time, a temperature variation of 1°C is also applied to the sensor. A linear relationship between R and glucose concentration is obtained for the tested concentration range. R remains unchanged for the three different temperatures within the given concentration range, which implies that R is insensitive to the ambient temperature

variability, and is only determined by the bulk refractive index of the glucose solution. However, the signals from through-port O_0 of the sensing ring are susceptible to the temperature variability and reduces the LOD. The calculated SNR is < 6.85 dB in the through-port O_0 and 19.88 dB after compensation within a 2°C temperature variation. The SNR is improved by 20 times in our chip compared to a single ring sensor. The linear relationship between R and peak shift $\Delta\lambda$ of the sensing ring from through port O_0 is also validated as shown in Figure S3. The results indicate that the wavelength interrogation approach widely used for single-ring sensor could be replaced by a low-cost intensity interrogation approach with our design without compromising the accuracy.

Biotoxoid Detection Results. The quantitative detection of botulinum toxoid type A is demonstrated following the procedure shown in Figure S4. The signals from output ports O_1 and O_2 are monitored by two photodetectors, and the signal from the output port O_0 is monitored by an OSA for comparison. Figure 5(b) shows the real-time testing results for 24 min. In the initial 2 min, the running buffer is injected into the microfluidic channel to form the baseline. The testing samples are then injected into the sensing chip for 20 min. Due to the fact that the refractive index of botulinum toxoid type A varies largely with concentration, the detected signals change substantially with botulinum toxoid type A of different concentrations. At this moment, the detected results (R values) correspond to the bulk refractive index sensing. The washing buffer is injected into the sensing chip at t = 22 min for 2 minutes to remove non-specific binding. True signals due to specific high-affinity binding are acquired at t = 24 min. The acquired R value versus target concentration is plotted in Figure 5(c) which shows a linear relationship. Figure 5(d) shows the temperature insensitive performance after the surface modification. R remains

almost a constant with a slope of only 0.01176 /°C as the temperature changes. The thermal drift significantly decreases by 28 times with compensation, and the effect of small temperature fluctuation is usually buried in the system noise. There are two factors contributing to the intensity instability. The first one can be attributed to the flow-induced transients, and the second one is due to Fabry-Perot reflections within the I/O grating couplers and at the interfaces between the silica upper-cladding and sensing medium in the sensing window. The coefficient of variation (CV) is used to evaluate the stability of the sensing system. Figure 4(a) shows that the CV is less than 0.216% for all conditions. The CVs of experiment results in Figures 5(c) and (d) are 0.531% and 0.338%, respectively. The small values almost entirely fall within the 95% prediction bands even with a 2°C temperature variation as shown in Figure 5(c).

Conclusions

In summary, a biotoxoid photonic sensor that is resistant to temperature fluctuation has been demonstrated. This novel sensor consists of a ring resonator coupled to an MZI readout unit. Instead of using costly wavelength interrogation, our photonic sensor directly measures the light intensity ratio between the two output ports of MZI. The TD controlling section of the MZI is used to eliminate the adverse effects of ambient temperature fluctuation. The simulation and experimental results show a linear relationship between the interrogation function and the concentration of analyte under operation conditions. The thermal drift of the proposed sensor is just 0.18%, which is a reduction of 567 folds for chemical sensing and 28 folds for immuno biosensing compared to conventional single ring resonator. The SNR increases from 6.85 dB to 19.88 dB within a 2°C temperature variation. The sensitivity of the designed biosensor with x = 2.43 is 0.21/decade, and its LOD is 1.69 ng/mL with a linear dynamic range from 55 ng/mL to 800 ng/mL. The CV of 0.531% shows a high accuracy. These performances make it comparable with other toxin detection work[36-37]. The high SNR optical sensor has a huge potential to push the LOD of biosensors to sub-picogram per milliliter range in combination with signal enhancement strategies[38]. Such a high sensitivity is critical for the detection of biotoxins which are often present at a low centration. It also promises great potential for amplification-free of detection of nucleic acids and other biomarkers[39-44].

Supporting Information

Supporting Information Available: The following files are available free of charge. SUPPLEMENTARY INFORMATION FOR A Biotoxoid Photonic Sensor with Temperature-Insensitivity Using Cascade of Ring Resonator and Mach-Zehnder Interferometer. Additional materials for more detailed experimental results of designed sensor under both chemical and biological sample solution. Further analysis about the relationship between the new and traditional signal, assisted information of detection process and simulation parameters used are also included.

Author Contributions

Z. Y. Li, J. Zou and A. Q. Liu jointly conceived the idea. Z. Y. Li, J. Zou and H. H. Zhu performed the numerical simulations and theoretical analysis. Z. Y. Li, J. Zou, B. T. T. Nguyen, R. C. Bailey, J. Zhou, H. Wang and H. Cai performed the fabrication and experiments. Z. Y. Li, J. Zou, Z. C. Yang, Y. F. Jin, P. H. Yap, Y. L. Hao and A. Q. Liu were involved in the discussion and data analysis. Z. Y. Li, J, Zou, Y. Z. Shi, P. Y. Liu and A. Q. Liu wrote the manuscript. Z. Y. Li and A. Q. Liu supervised and coordinated all of the work.

Notes

The authors declare no competing financial interest.

Acknowledgement

This work was supported by the Singapore National Research Foundation under the Competitive Research Program (NRF-CRP13-2014-01), EWI Research & Innovation Scheme (1102-IRIS-05-04), the Singapore Ministry of Education (MOE) Tier 3 grant (MOE2017-T3-1-001), and the National Science Foundation of China under Grant 61605172.

References

1. Sun, Y.; Fan, X., Optical ring resonators for biochemical and chemical sensing. *Analytical and Bioanalytical Chemistry* **2011,** *399* (1), 205-211.
2. Fan, X.; White, I. M.; Shopova, S. I.; Zhu, H.; Suter, J. D.; Sun, Y., Sensitive optical biosensors for unlabeled targets: A review. *Analytica Chimica Acta* **2008,** *620* (1), 8-26.
3. Ciminelli, C.; Campanella, C. M.; Dell'Olio, F.; Campanella, C. E.; Armenise, M. N., Label-free optical resonant sensors for biochemical applications. *Progress in Quantum Electronics* **2013,** *37* (2), 51-107.
4. Janz, S.; Xu, D. X.; Vachon, M.; Sabourin, N.; Cheben, P.; McIntosh, H.; Ding, H.; Wang, S.; Schmid, J. H.; Delâge, A.; Lapointe, J.; Densmore, A.; Ma, R.; Sinclair, W.; Logan, S. M.; MacKenzie, R.; Liu, Q. Y.; Zhang, D.; Lopinski, G.; Mozenson, O.; Gilmour, M.; Tabor, H., Photonic wire biosensor microarray chip and instrumentation with application to serotyping of Escherichia coliisolates. *Optics Express* **2013,** *21* (4), 4623-4637.
5. Cardenosa-Rubio, M. C.; Robison, H. M.; Bailey, R. C., Recent advances in environmental and clinical analysis using microring resonator–based sensors. *Current Opinion in Environmental Science & Health* **2019**.
6. Wade, J. H.; Bailey, R. C., Applications of Optical Microcavity Resonators in Analytical Chemistry. *Annual Review of Analytical Chemistry* **2016,** *9* (1), 1-25.
7. Chen, Y.; Liu, J.; Yang, Z.; Wilkinson, J. S.; Zhou, X., Optical biosensors based on refractometric sensing schemes: A review. *Biosensors and Bioelectronics* **2019,** *144*, 111693.

8. Kindt, J. T.; Bailey, R. C., Biomolecular analysis with microring resonators: applications in multiplexed diagnostics and interaction screening. *Current Opinion in Chemical Biology* **2013,** *17* (5), 818-826.

9. Shi, Y.; Zhao, H.; Nguyen, K. T.; Zhang, Y.; Chin, L. K.; Zhu, T.; Yu, Y.; Cai, H.; Yap, P. H.; Liu, P. Y.; Xiong, S.; Zhang, J.; Qiu, C.-W.; Chan, C. T.; Liu, A. Q., Nanophotonic Array-Induced Dynamic Behavior for Label-Free Shape-Selective Bacteria Sieving. *ACS Nano* **2019,** *13* (10), 12070-12080.

10. Song, J.; Luo, X.; Tu, X.; Park, M. K.; Kee, J. S.; Zhang, H.; Yu, M.; Lo, G.-Q.; Kwong, D.-L., Electrical tracing-assisted dual-microring label-free optical bio/chemical sensors. *Optics Express* **2012,** *20* (4), 4189-4197.

11. Chen, Y.; Yu, F.; Yang, C.; Song, J.; Tang, L.; Li, M.; He, J.-J., Label-free biosensing using cascaded double-microring resonators integrated with microfluidic channels. *Optics Communications* **2015,** *344*, 129-133.

12. Zhang, Y.; Zou, J.; He, J.-J., Temperature sensor with enhanced sensitivity based on silicon Mach-Zehnder interferometer with waveguide group index engineering. *Optics express* **2018,** *26* (20), 26057-26064.

13. Jiang, X.; Ye, J.; Zou, J.; Li, M.; He, J.-J., Cascaded silicon-on-insulator double-ring sensors operating in high-sensitivity transverse-magnetic mode. *Optics Letters* **2013,** *38* (8), 1349-1351.

14. Jiang, X.; Chen, Y.; Yu, F.; Tang, L.; Li, M.; He, J.-J., High-sensitivity optical biosensor based on cascaded Mach-Zehnder interferometer and ring resonator using Vernier effect. *Optics Letters* **2014,** *39* (22), 6363-6366.

15. Feng, X.; Zhang, G.; Chin, L. K.; Liu, A. Q.; Liedberg, B., Highly Sensitive, Label-Free Detection of 2,4-Dichlorophenoxyacetic Acid Using an Optofluidic Chip. *ACS Sensors* **2017,** *2* (7), 955-960.

16. Xu, D. X.; Vachon, M.; Densmore, A.; Ma, R.; Janz, S.; Delâge, A.; Lapointe, J.; Cheben, P.; Schmid, J. H.; Post, E.; Messaoudène, S.; Fédéli, J.-M., Real-time cancellation of temperature induced resonance shifts in SOI wire waveguide ring resonator label-free biosensor arrays. *Optics Express* **2010,** *18* (22), 22867-22879.

17. Lee, J.; Kim, D.; Ahn, H.; Park, S.; Kim, G., Temperature Dependence of Silicon Nanophotonic Ring Resonator With a Polymeric Overlayer. *Journal of Lightwave Technology* **2007,** *25* (8), 2236-2243.

18. Washburn, A. L.; Shia, W. W.; Lenkeit, K. A.; Lee, S.-H.; Bailey, R. C., Multiplexed cancer biomarker detection using chip-integrated silicon photonic sensor arrays. *Analyst* **2016,** *141* (18), 5358-5365.

19. Valera, E.; Shia, W. W.; Bailey, R. C., Development and validation of an immunosensor for monocyte chemotactic protein 1 using a silicon photonic microring resonator biosensing platform. *Clinical Biochemistry* **2016,** *49* (1), 121-126.

20. Luchansky, M. S.; Bailey, R. C., High-Q Optical Sensors for Chemical and Biological Analysis. *Analytical Chemistry* **2012,** *84* (2), 793-821.

21. Zou, J.; Le, Z.; He, J., Temperature Self-Compensated Optical Waveguide Biosensor Based on Cascade of Ring Resonator and Arrayed Waveguide Grating Spectrometer. *Journal of Lightwave Technology* **2016,** *34* (21), 4856-4863.

22. Xie, Z.; Cao, Z.; Liu, Y.; Zhang, Q.; Zou, J.; Shao, L.; Wang, Y.; He, J.; Li, M., Highly-sensitive optical biosensor based on equal FSR cascaded microring resonator with intensity interrogation for detection of progesterone molecules. *Optics Express* **2017,** *25* (26), 33193-33201.

23. Bogaerts, W.; De Heyn, P.; Van Vaerenbergh, T.; De Vos, K.; Kumar Selvaraja, S.; Claes, T.; Dumon, P.; Bienstman, P.; Van Thourhout, D.; Baets, R., Silicon microring resonators. *Laser & Photonics Reviews* **2012,** *6* (1), 47-73.

24. Shi, Y. Z.; Xiong, S.; Chin, L. K.; Yang, Y.; Zhang, J. B.; Ser, W.; Wu, J. H.; Chen, T. N.; Yang, Z. C.; Hao, Y. L.; Liedberg, B.; Yap, P. H.; Zhang, Y.; Liu, A. Q., High-resolution and multi-range particle separation by microscopic vibration in an optofluidic chip. *Lab on a Chip* **2017,** *17* (14), 2443-2450.

25. Kokubun, Y.; Yoneda, S.; Matsuura, S., Temperature-independent optical filter at 1.55um wavelength using a silica-based athermal waveguide. *Electronics Letters* **1998,** *34* (4), 367-369.

26. Okada, Y.; Tokumaru, Y., Precise determination of lattice parameter and thermal expansion coefficient of silicon between 300 and 1500 K. *Journal of Applied Physics* **1984,** *56* (2), 314-320.

27. Barrios, C. A., Integrated microring resonator sensor arrays for labs-on-chips. *Analytical and Bioanalytical Chemistry* **2012,** *403* (6), 1467-1475.

28. Shi, Y.; Xiong, S.; Chin, L. K.; Zhang, J.; Ser, W.; Wu, J.; Chen, T.; Yang, Z.; Hao, Y.; Liedberg, B.; Yap, P. H.; Tsai, D. P.; Qiu, C.-W.; Liu, A. Q., Nanometer-precision linear sorting with synchronized optofluidic dual barriers. *Science Advances* **2018,** *4* (1), eaao0773.

29. Shi, Y. Z.; Xiong, S.; Zhang, Y.; Chin, L. K.; Chen, Y. Y.; Zhang, J. B.; Zhang, T. H.; Ser, W.; Larrson, A.; Lim, S. H.; Wu, J. H.; Chen, T. N.; Yang, Z. C.; Hao, Y. L.; Liedberg, B.; Yap, P. H.; Wang, K.; Tsai, D. P.; Qiu, C. W.; Liu, A. Q., Sculpting nanoparticle dynamics for single-bacteria-level screening and direct binding-efficiency measurement. *Nature Communications* **2018,** *9* (1), 815.

30. Shi, Y.; Zhu, T.; Zhang, T.; Mazzulla, A.; Tsai, D. P.; Ding, W.; Liu, A. Q.; Cipparrone, G.; Sáenz, J. J.; Qiu, C.-W., Chirality-assisted lateral momentum transfer for bidirectional enantioselective separation. *Light: Science & Applications* **2020,** *9* (1), 1-12.

31. Lee, H.-S.; Kim, G.-D.; Lee, S.-S., Temperature compensated refractometric biosensor exploiting ring resonators. *IEEE Photonics Technology Letters* **2009,** *21* (16), 1136-1136.

32. Wade, J. H.; Bailey, R. C., Refractive Index-Based Detection of Gradient Elution Liquid Chromatography using Chip-Integrated Microring Resonator Arrays. *Analytical Chemistry* **2014,** *86* (1), 913-919.

33. Robison, H. M.; Bailey, R. C., A Guide to Quantitative Biomarker Assay Development using Whispering Gallery Mode Biosensors. In *Current Protocols in Chemical Biology*, John Wiley & Sons, Inc.: 2009.

34. Zhu, X.; Wang, R.; Zhou, X.; Shi, H., Free-Energy-Driven Lock/Open Assembly-Based Optical DNA Sensor for Cancer-Related microRNA Detection with a Shortened Time-to-Result. *ACS Applied Materials & Interfaces* **2017,** *9* (31), 25789-25795.

35. Long, F.; Gu, C.; Gu, A. Z.; Shi, H., Quantum Dot/Carrier–Protein/Haptens Conjugate as a Detection Nanobioprobe for FRET-Based Immunoassay of Small Analytes with All-Fiber Microfluidic Biosensing Platform. *Analytical Chemistry* **2012,** *84* (8), 3646-3653.

36. Liu, L.-h.; Zhou, X.-h.; Shi, H.-c., Portable optical aptasensor for rapid detection of mycotoxin with a reversible ligand-grafted biosensing surface. *Biosensors and Bioelectronics* **2015,** *72*, 300-305.

37. Liu, L.; Shan, D.; Zhou, X.; Shi, H.; Song, B.; Falke, F.; Leinse, A.; Heideman, R., TriPleX™ waveguide-based fluorescence biosensor for multichannel environmental contaminants detection. *Biosensors and Bioelectronics* **2018,** *106*, 117-121.

38. Kindt, J. T.; Luchansky, M. S.; Qavi, A. J.; Lee, S.-H.; Bailey, R. C., Subpicogram Per Milliliter Detection of Interleukins Using Silicon Photonic Microring Resonators and an Enzymatic Signal Enhancement Strategy. *Analytical Chemistry* **2013,** *85* (22), 10653-10657.

39. Mordan, E. H.; Wade, J. H.; Wiersma, Z. S. B.; Pearce, E.; Pangburn, T. O.; deGroot, A. W.; Meunier, D. M.; Bailey, R. C., Silicon Photonic Microring Resonator Arrays for Mass Concentration Detection of Polymers in Isocratic Separations. *Analytical Chemistry* **2019,** *91* (1), 1011-1018.

40. Graybill, R. M.; Para, C. S.; Bailey, R. C., PCR-Free, Multiplexed Expression Profiling of microRNAs Using Silicon Photonic Microring Resonators. *Analytical Chemistry* **2016,** *88* (21), 10347-10351.

41. Wade, J. H.; Alsop, A. T.; Vertin, N. R.; Yang, H.; Johnson, M. D.; Bailey, R. C., Rapid, Multiplexed Phosphoprotein Profiling Using Silicon Photonic Sensor Arrays. *ACS Central Science* **2015,** *1* (7), 374-382.

42. McClellan, M. S.; Domier, L. L.; Bailey, R. C., Label-free virus detection using silicon photonic microring resonators. *Biosensors and Bioelectronics* **2012,** *31* (1), 388-392.

43. Kindt, J. T.; Bailey, R. C., Chaperone Probes and Bead-Based Enhancement To Improve the Direct Detection of mRNA Using Silicon Photonic Sensor Arrays. *Analytical Chemistry* **2012,** *84* (18), 8067-8074.

44. Shia, W. W.; Bailey, R. C., Single Domain Antibodies for the Detection of Ricin Using Silicon Photonic Microring Resonator Arrays. *Analytical Chemistry* **2013,** *85* (2), 805-810.

Figures

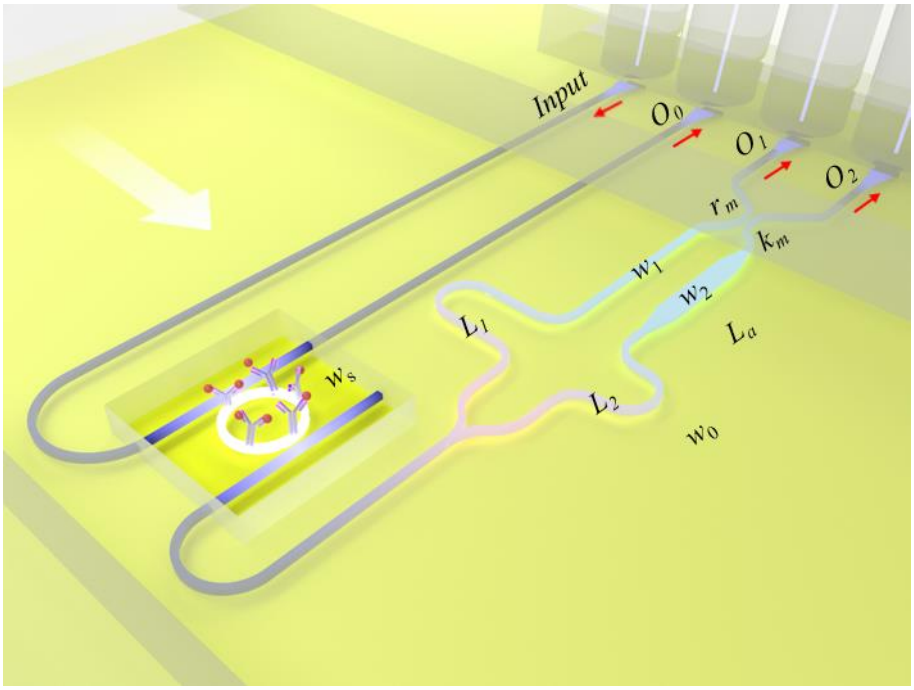

(a)

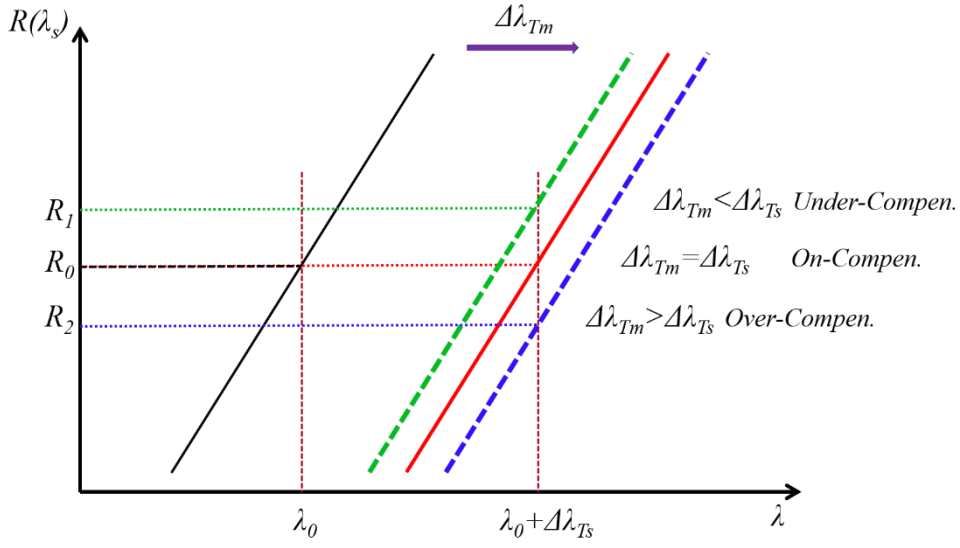

(b)

Figure 1. Device architecture and principle for the proposed temperature-insensitive photonic sensor. (a) Detailed view of the proposed sensor structure and rough operating

situation with related parameters labeled in. (b) Schematic illustration of the temperature-insensitive detection principle for the sensing ring as the environmental temperature has a small variation of ΔT. $\Delta\lambda_{Ts}$ represents the temperature change induced resonance wavelength shift of the sensing ring resonator and $\Delta\lambda_{Tm}$ spectral shift of the MZI. Only when $\Delta\lambda_{Tm}$ is equal to $\Delta\lambda_{Ts}$, the value of $R(\lambda_s)$ remains unchanged, named as on-compensation condition.

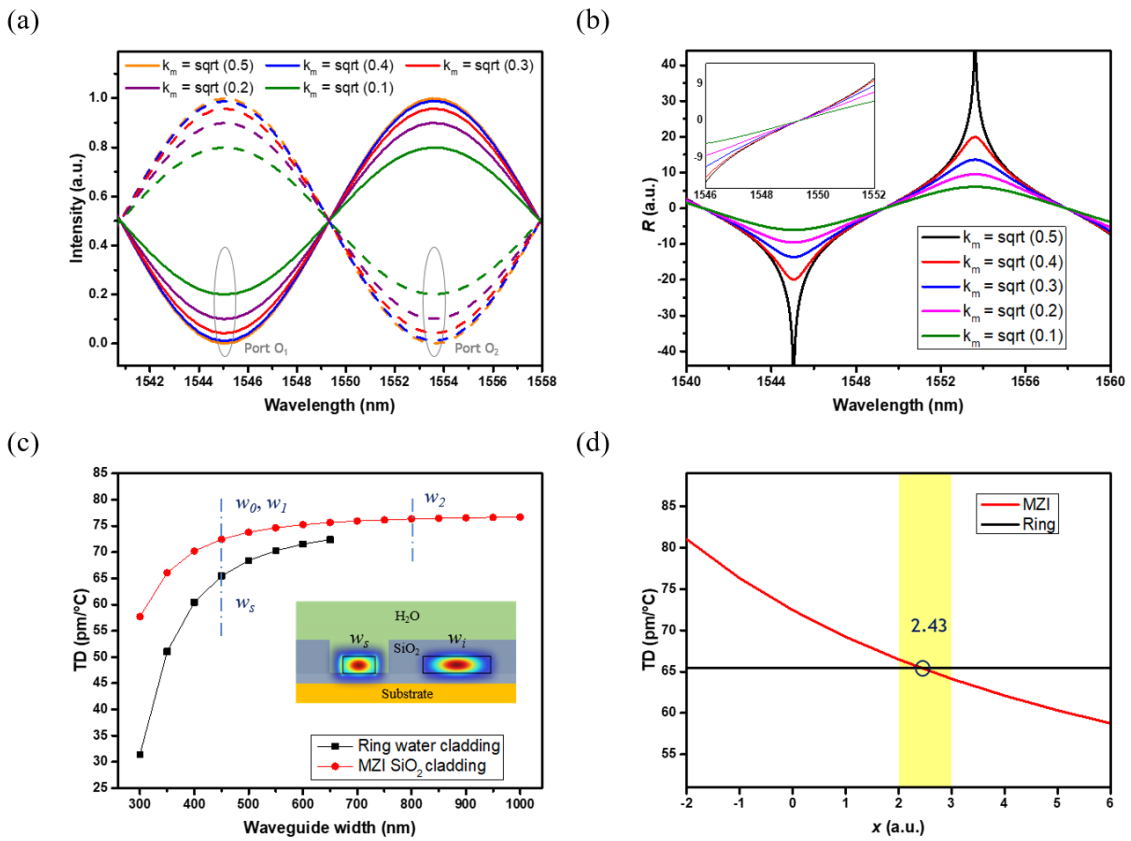

Figure 2. Simulation results of the output curve with different DC parameter and TD versus waveguide width. (a) Spectral responses of the two output ports O_1 and O_2 of the MZI with different cross-coupling coefficient k_m, respectively. The output DC of the MZI has a waveguide width of w_0 = 450 nm and gap of 200 nm in the simulation, and different coupling length corresponds to different cross-coupling coefficient k_m. (b) R as a function of λ with different k_m values of $\sqrt{0.1}$, $\sqrt{0.2}$, $\sqrt{0.3}$, $\sqrt{0.4}$, $\sqrt{0.5}$, respectively and its close-up at the wavelength around 1550 nm. (c) TDs of the fundamental TE mode with respect to the width of a waveguide (as shown in the lower-right) with water and silica as its upper-cladding respectively, at the wavelength of 1.55 μm. The determined waveguide widths w_i (i = 0,1,2) for the MZI, and the ring width w_s, are also indicated. (d) TD of the MZI as a function of the compensation factor x at the wavelength of 1.55 μm based on

the parameters given in Table S1. The required value for x to make the TD of the MZI equal to that of the ring sensor is ~2.43.

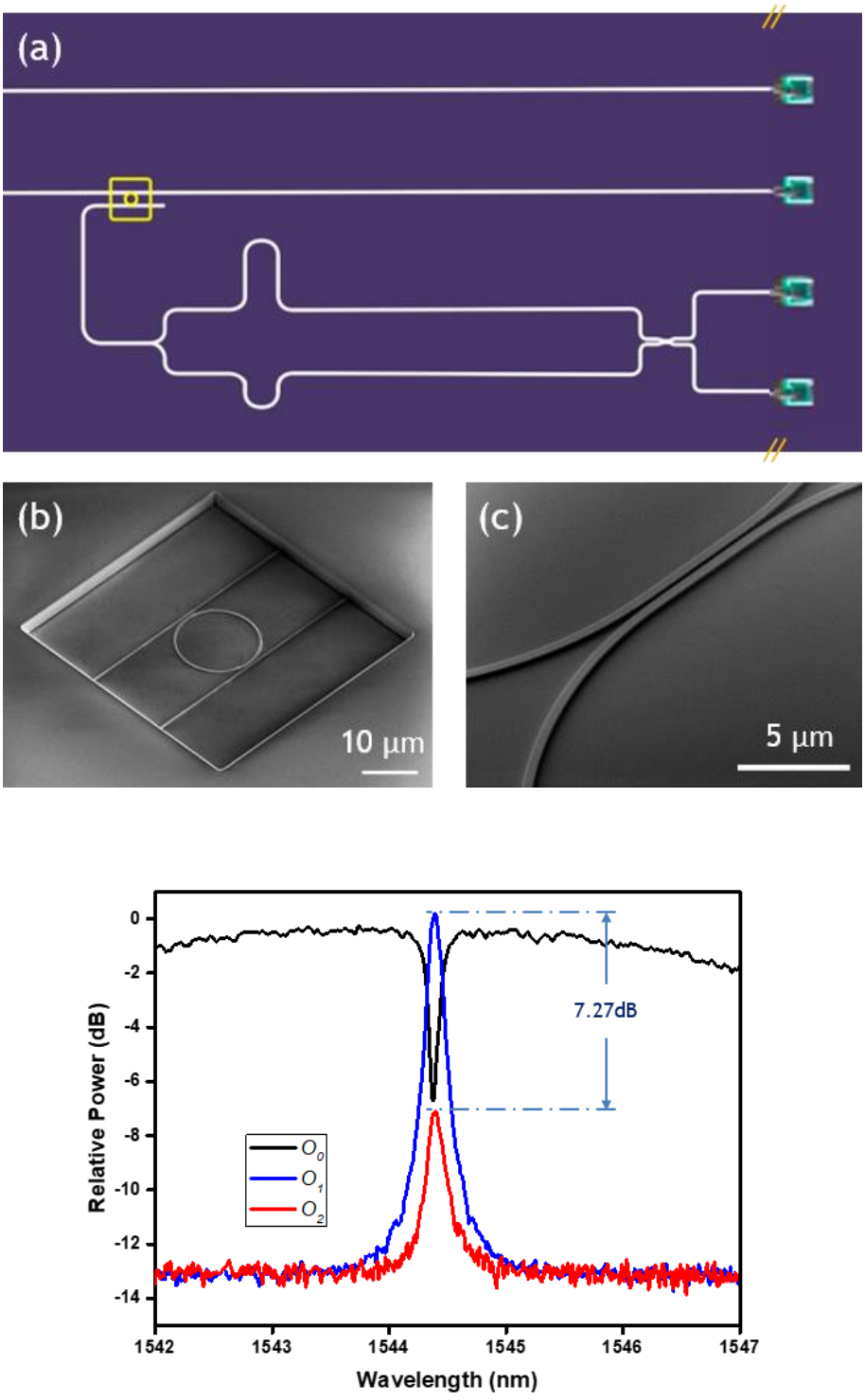

(d)

Figure 3. Micrograph of the sensor and its spectral response. (a) Optical micrograph of chip that shows the sensing window and MZI region (sharpened and false-colored to

show the key features). The output waveguides between DC and grating coupler are cropped. The original micrograph is available in Figure S1(a). (b) Electron micrograph of the sensing window. (c) Electron micrograph of the directional coupler (taken before the cladding material is deposited). (d) Three outputs performance of temperature insensitive sensor within one peak by external bandwidth-variable tunable filter.

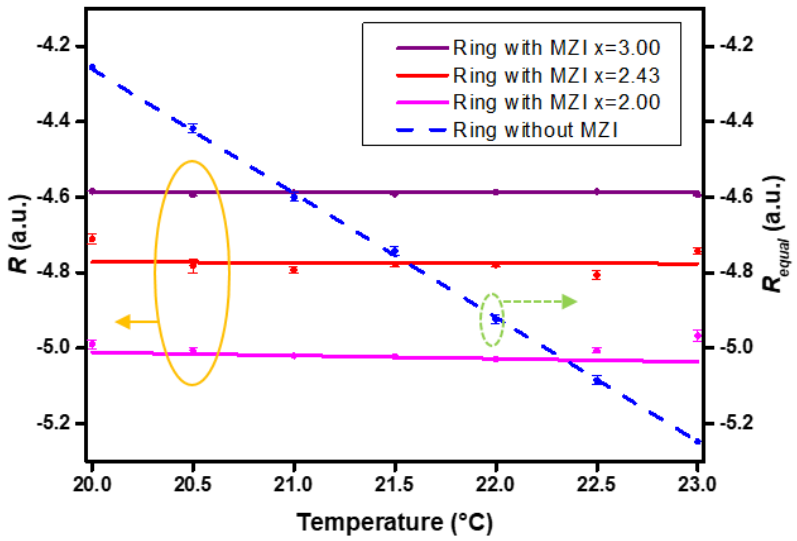

(a)

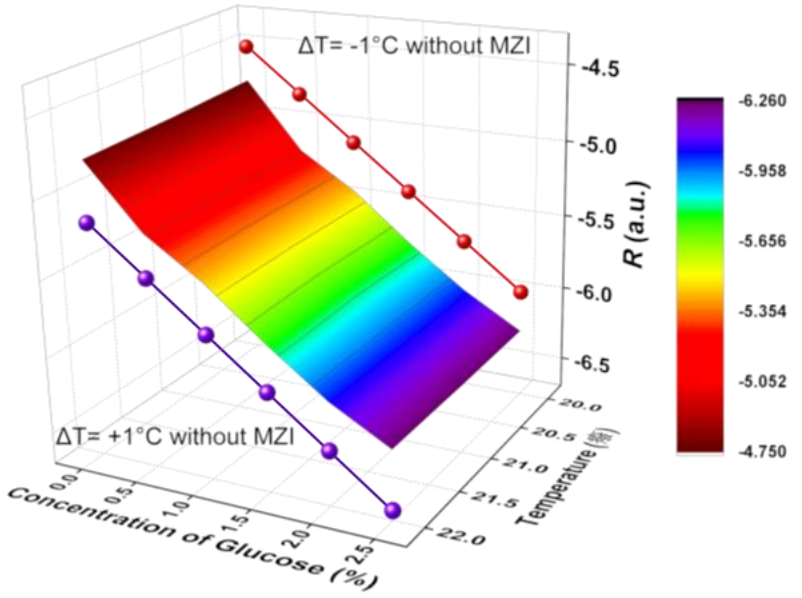

(b)

Figure 4. Experimental results of the fabricated sensor chip under glucose solution. (a) Measurement results of the sensor chip under three different *x* values of 2, 2.43 and 3 by varying the temperature. The slopes are 0.00058 /°C, 0.00139 /°C and 0.0084/°C for *x* = 3, 2.43 and 2, respectively, while that is 0.329 /°C for the output port O_0 corresponding to

the single ring detection. (b) The experimentally detected *R* as a function of the cladding solution at three different environmental temperatures with and without MZI.

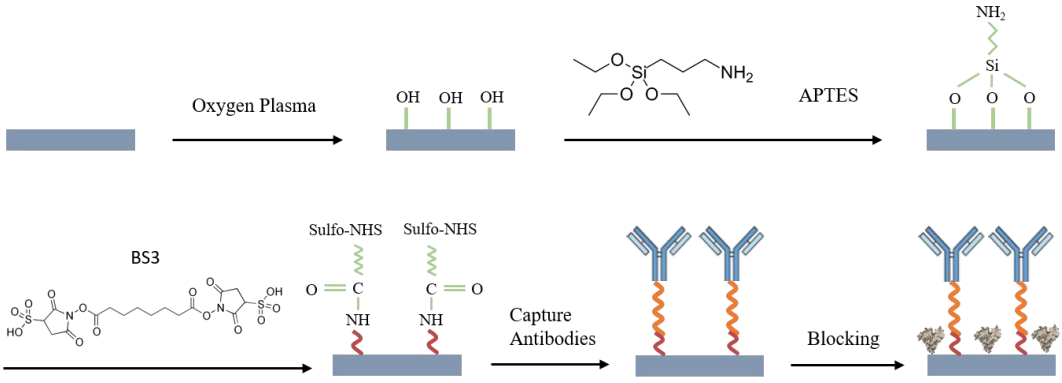
Oxygen Plasma
OH OH OH
APTES
NH2
Si
O O O
BS3
Sulfo-NHS
Sulfo-NHS
C O
NH
Capture
Antibodies
Blocking

(a)

(b)

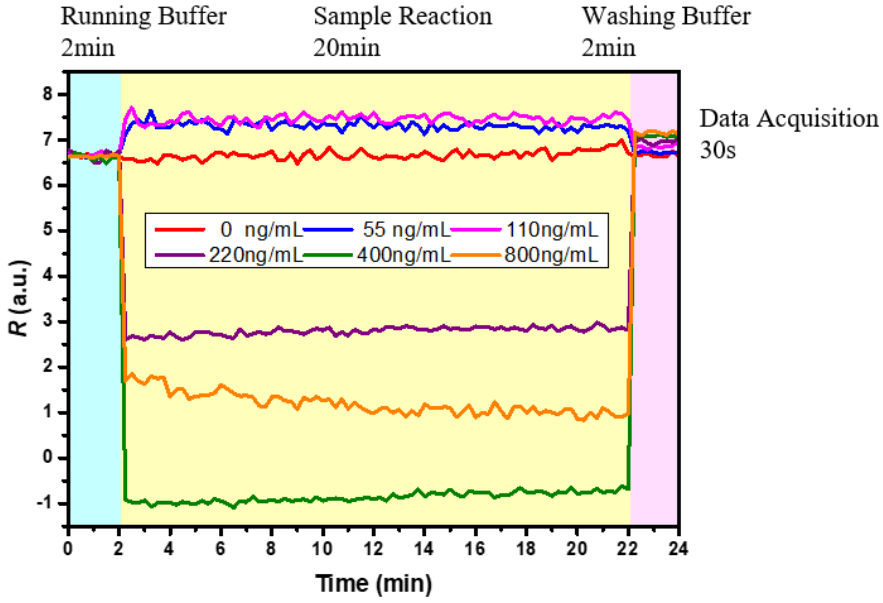
Running Buffer
2min
Sample Reaction
20min
Washing Buffer
2min
Data Acquisition
30s
0 ng/mL
55 ng/mL
110ng/mL
220ng/mL
400ng/mL
800ng/mL
R (a.u.)
Time (min)

(c)

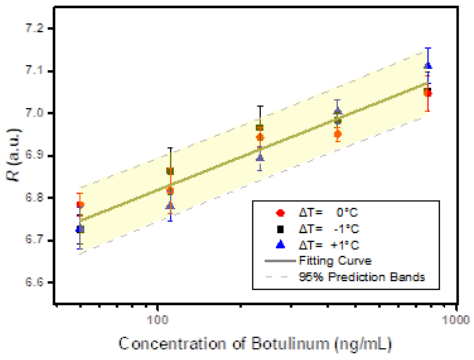
ΔT= 0°C
ΔT= -1°C
ΔT= +1°C
Fitting Curve
95% Prediction Bands
R (a.u.)
Concentration of Botulinum (ng/mL)

(d)

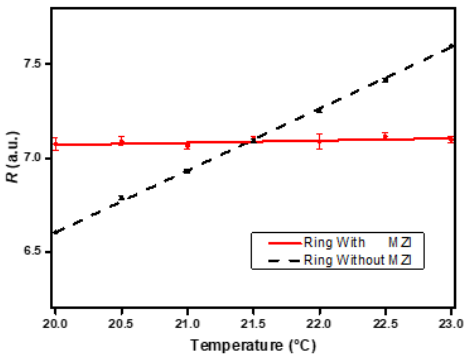
Ring With MZI
Ring Without MZI
R (a.u.)
Temperature (°C)

Figure 5. Experimental results of the sensor chip for the detection of botulinum toxoid type A. (a) Surface modification protocol of the biotoxoid sensor chip functionalized with the capture antibody. (b) The evolution of R in dynamic period under different concentrations of botulinum toxoid type A through the monitor for the ports O_1 and O_2. (c) R as a function of the concentration of botulinum toxoid type A at three different environmental temperatures with MZI. (d) Temperature influence testing for the sensor chip.

Table 1: Simulated results for the fundamental TE modes of the ring resonator and MZI waveguides at the wavelength of 1.55μm. The waveguide height is 220nm.

Parameter	**Ring WG (water cladding)**	**MZI WG (silica cladding)**		
	w_s **(450nm)**	w_0 **(450nm)**	w_1 **(450nm)**	w_2 **(800nm)**
TD (pm/°C)	65.44	72.45	72.45	76.32
n_{eff}	2.3247	2.3517	2.3517	2.6889
$\partial n_{eff}/\partial T$ (1/°C)	1.85×10^{-4}	2.01×10^{-4}	2.01×10^{-4}	1.93×10^{-4}
n_g	4.3877	4.3088	4.3088	3.9207

For TOC Only